OPEN ○ ACCESS

UNIVERSITY OF THE
WEST *of* SCOTLAND
UWS

UWS Academic Portal

Development of a metal matrix composite layer on a microalloyed steel surface by dissociating MAX211 Ti2AlC particles using a TIG torch technique

Munoz De Escalona, Patricia; Lees, Christopher; Sillars, Fiona; Mridha, Shahjahan; Baker, Thomas

Link to publication on the UWS Academic Portal

Download date: 17 Sep 2019

Development of a metal matrix composite layer on a microalloyed steel surface by dissociating MAX211 Ti$_2$AlC particles using a TIG torch technique

P. Muñoz de Escalona[1], C. Lees[2], F.Sillars[2], S. Mridha[2] and T. N. Baker[2]

[1] School of Engineering and Computing
University of the West of Scotland,
Paisley, PA1 2BE, UK.

[2] Department of Mechanical and Aerospace Engineering
University of Strathclyde,
Glasgow G1 1XJ, UK.

*Corresponding author: p.munoz@uws.ac.uk

Abstract

A surface engineering method utilised a tungsten inert gas torch to melt a preplaced MAX211, Ti$_2$AlC powder particles into a microalloyed steel substrate with the aim of producing a surface metal matrix composite.. In this study, the two different shielding gases, argon and a mixture of argon + helium (80% + 20%), were used to protect the surfaces under different processing conditions, with the aim of finding the optimal conditions for further studies. An analysis of the morphology, microstructure and hardness profile of the melted zone, showed that in general, samples melted under argon achieved a higher hardness and exhibited a smaller penetration into the substrate compared to melting under a mixture of argon + helium. An XRD study showed that the Ti$_2$AlC powder decomposed to TiC particles dispersed in mainly TiAl.

Keywords: surface engineering, TIG, argon, helium, hardness, Ti$_2$AlC

1. Introduction

Research on metal matrix composites (MMC's) has developed significantly, including enhancing surface properties, due to their technological and commercial significance. The broad range of use of MMC's within industries, includes ground (road and rail) and air transportation, thermal management, recreational and infrastructure. Furthermore, the advantages of the properties of MMC's, such as high thermal and electrical conductivity,

good resistance to aggressive environments, good impact and erosion resistance, have been reported [1, 2].

The increased attention given to the Ti_2AlC, whose properties bridge the gap between a metal and a ceramic, is a result of the attractive properties it possesses [3]. Ti_2AlC is part of a wider group of ternary carbides and nitrides known as MAX phases, so named due to their chemical formula: $M_{n+1}AX_n$ where n=1,2 or 3, M is a transition metal, A is from the 13-16 group of elements and X is carbon and/or nitrogen. According to Barsoum and Radovic [3], the boom in development of this type of material since the early 1990's is due to the unusual, sometimes unique combination of parameters they display. Parameters specific to Ti_2AlC are discussed by Zhuo et al [4], and include characteristics such as good machinability, low density, good electrical and thermal conductivity, and high-temperature oxidation resistance. It is the most oxidation resistant of the MAX phases, because it forms a stable and protective layer of Al_2O_3. These are all attractive properties in the context of manufacturing components, and the development of a Ti_2AlC MMC surface coating has been relatively easy to facilitate for aluminium and titanium alloys, [3], improving the surface characteristics of the host surface. This research[3,4] also emphasised the key mechanical properties which are improved by Ti_2AlC surface coatings, such as strength, creep resistance, and fracture toughness; which means that just a thin composite layer can have a significant effect on a surface. This conclusion is supported by a similar study carried out by Mei et al (2007) [5], which reached the same conclusions regarding Ti_2AlC.They also state that they believe Ti_2AlC is the most promising of the MAX phase metals for high temperature applications on account of a low cost of raw materials, low density, and excellent oxidation performance which is independent of thermal cycling. The fact that Ti_2AlC is able to withstand very high levels of thermal shock may allow its use in a tungsten inert gas (TIG) welding process where other materials may not be able to withstand the high temperatures, causing them to deteriorate. However, Ti_2AlC is known to decompose above 1450°C by sublimation of Ti and Al, to TiC [6], so the processing conditions will differ from the application of TIG to develop surface MMC,s incorporating ceramic powders such as TiC or SiC [7,8]

The tungsten inert gas (TIG) process involves an electrical arc being created between a non-consumable tungsten electrode and the work surface. Weman [9] studied the TIG process in more detail, describing how an inert gas, usually argon or a combination of argon with another gas, is used to protect the weld pool and electrode. This is normally supplied through a gas cup at the end of the welding torch, in the middle of which the electrode is positioned.

Weman cites the main advantages of choosing TIG as having a very stable arc and excellent control of the finished welding result.

Another key parameter in the welding process is the choice of shielding gas, as this has an influence on the welding arc itself, and on the quality of the welds produced. Tashira et al [10] have discussed the variety of shielding gases available, and have highlighted that the inertness and relatively low cost of argon are why it is still the most widely used gas. However, it suffers slightly from a lower heat flux transferred to the substrate, and as a result, helium, mixtures of argon with helium, and also nitrogen may be utilised. Considering the use of argon by itself, it is expected that the melt depth will be less compared to the use of other shielding gases, or a combination of them. The study also highlighted the pitfalls of adding different gases to argon, where introduction of contaminants and the increase of defects such as porosity were mentioned. [10]

Very similar studies detailing the procedure of using a TIG torch to initiate a MMC melting process are to date fairly sparse as this is an emerging area of study. Dyuti et al [11] used Ti-Al powder melted onto a mild steel surface to produce an MMC, and concluded that the maximum surface hardness can be increased by up to five times, depending on parameters such as the energy input. The results also showed that when the energy input was increased to 675 J/mm, the hardness abruptly decreased and remained constant along the melt depth, suggesting that the hardness of the coating layer also depends on the energy density of the TIG torch. This of course implies that in this work [12] the higher the energy density (heat input), the lower the hardness of the welded surface.

To date, little has been published on incorporating MAX phases composites. Shi et al [13] have a developed a $TiC/Ti_2AlC/TiAl_3$ in situ ceramic/MAX phase composite. The present research, has as the main aim, obtaining the optimal conditions regarding the geometry and hardness for the development of an MMC on the surface of a microalloyed steel substrate using Ti_2AlC when using a TIG process. A secondary objective is to analyse the surface composition, following a series of energy inputs, to determine the phases present on the re-solidified surface. The results will determine the path of future work.

2. Experimental Procedure

2.1. Workpiece characteristics

Microalloyed steel plates with dimensions 300 x 30 x 10 mm and composition 0.1C-0.7Mn-0.05Cu-0.05Nb (all in wt%) were used for the experiment. The chemical composition of the

microalloyed steel substrate was determined using a Glow Discharge Optical Emission Spectrometer model Horiba GD-OES profilometer.

The substrate was divided into six sections of 40 x 30 x 10 mm with 1mm gap left between each section. 3gr of Ti_2AlC, supplied as 80% ≤ 20μm size MAXthal 211 powder, by Sandvik Materials Technology ,was used to cover the 300 x 30 mm^2 steel subsurface. Figure 1 shows a schematic drawing of the sample.

Once the melting process was completed, the samples were allowed to cool to room temperature for microstructural determination and microhardness analysis.
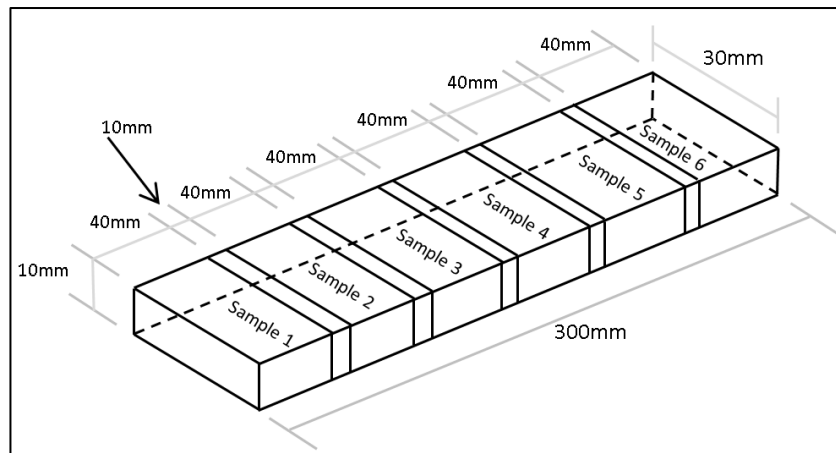

Figure 1 Schematic drawing of the samples dimensions

2.2. Shielding gases characteristics

A comparison of the effect of two shielding gases, argon and argon + helium mixture (80% + 20%) on surface microstructure and hardness profiles. The properties are collated in Table 1.

Table 1. Thermal properties of the shielding gases used in this research

Property	Argon (14CL)	Helium(15CL)
Density [Kg/m^3]	1.661	0.169
Specific heat [kJ /Kg K]	0.520	5.190
Thermal conductivity [W/m K]	0.016	0.143
First ionization potential [eV]	15.8	24.58

2.3 Ceramic particles

Titanium aluminium carbide (Ti_2AlC) was selected for this study as it is known to improve the strength, fracture toughness and creep resistance of a surface with just a thin layer [5].

Here we are looking to develop a functionally graded layer of ~1mm thickness. Table 2 shows properties of the Ti_2AlC characterised as follows:

Table 2 Ti_2AlC properties [9]

Density (kg/m^3)	94200
Fracture Strength (MPa)	370
Hardness (HV)	285
Fracture Toughness (MPa m$^{1/2}$)	5.2

2.4. Equipment characteristics

A Miller Dynastry 300DX TIG equipment was used to generate an arc with a 2.4 mm diameter thoriated tungsten electrode. The tungsten electrode was direct current negative and the tip of the electrode was placed 1 mm above the sample's surface.

2.5. Melting conditions and temperature registration

Different energy inputs conditions were obtained through the combination of the energy input parameters. Tables 3 and 4 show the different energy inputs used in this investigation using different shielding gases.

The energy input was calculated using equation 1.

$$E = \eta \frac{VI}{s} \qquad (1)$$

where:

η : efficiency of energy absorption (48% for a TIG process)

V: voltage (v)

I: Arc current (A)

s: welding speed (mm/s)

Tables 3 and 4 shows the parameters used.

Table 3 - Experimental parameters for samples using argon as shielding gas

Sample No.	I (A)	V(v)	s(mm/s)	E(J/mm)
1	60	11.0	0.5	630
2	80	12.0	0.5	900
3	100	13.0	0.5	1200
4	80	12.0	1.0	450
5	90	12.0	1.0	500
6	100	12.5	1.0	600

Table 4 - Experimental parameters for samples using argon + helium as shielding gas

Sample No.	I (A)	V(v)	s(mm/s)	E (J/mm)
1	80	11.7	0.5	900
2	90	11.0	0.5	1000
3	100	12.5	0.5	1200
4	80	12.0	1.0	450
5	90	11.0	1.0	500
6	100	12.5	1.0	600

2.6. Metallography

To reveal the parent microstructure and that obtained after the melting process, metallographic techniques were conducted following ASTM E3-01 standards.

Chemical analysis of compounds developed in the re-solidified surface were obtained by X-ray diffraction, which was carried out in a Bruker D8 Advance with Da Vinci. A Cu (λ = 1.5406 Å) source x-ray tube was used. The x-ray tube was set to 40kV and 40mA. The step size was set to 0.5 seconds and the increment was set to 0.02°.The 2-theta range measured was 20 -90°. The spectra obtained were matched against compounds in the International Centre for Diffraction Data (ICDD) PDF-2 database. An Olympus GX51 optical microscope and a Hitachi S-3700 N scanning electron microscope (SEM) with an Oxford Instruments INCA system with 80 mm XMAX SDD detector were used to observe and chemically analyse the microstructure of the metallographic specimens.

2.7 Microhardness test

The microhardness measurements were conducted using a Mitutoyo MVK G1 microhardness tester with 200gf and 15s delay and following the procedures BS6507-1 1998 and BS 1043-2 1993. Figure 2 shows the pattern used for the microhardness reading on the specimen cross-section of melted zone (MZ), heat affected zone (HAZ) and parent material (PM), starting at 0.1 mm from the melted zone edge, and taking measurements in a vertical distance at 0.2 mm apart towards the centre of the specimen (parent material).
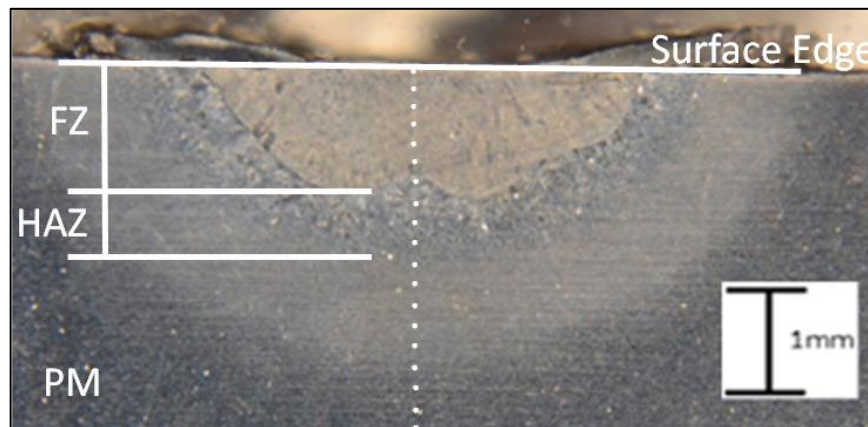
Figure 2. Pattern of microhardness indents taken on cross- sectional area of melted track.

3. Results and Discussion

3.1 Argon as shielding gas

Figure 3 shows the cross-sectional area of the melted track when using pure argon as the shielding gas at different energy inputs and a constant welding speed of 0.5mm/s.
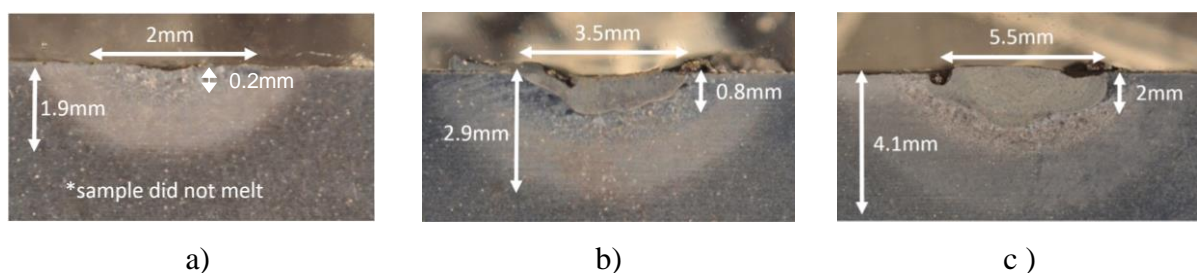

Figure 3 - Dimensions of melted track cross sectional area for samples welded at 0.5 mm/s using argon as shielding gas a) E=630J/mm, b) E=900J/mm, and c) E=1200J/mm

As observed when analysing Figure 3, the cross-sectional area increased when the energy input increased; an increase of 33% of the energy input (from 900J/mm to 1200J/mm) produced an increase of 57% of the width and 150% of the depth of the fusion zone respectively. However when detailing each of the sections, it is observed that the top of the melted zone was concave for E<900 J/mm, and in general that most of the material has being skewed to the side of the fusion zone.

Figure 4 shows the cross-sectional area when using pure argon as shielding gas at different energy inputs and a constant welding speed of 1.0mm/s
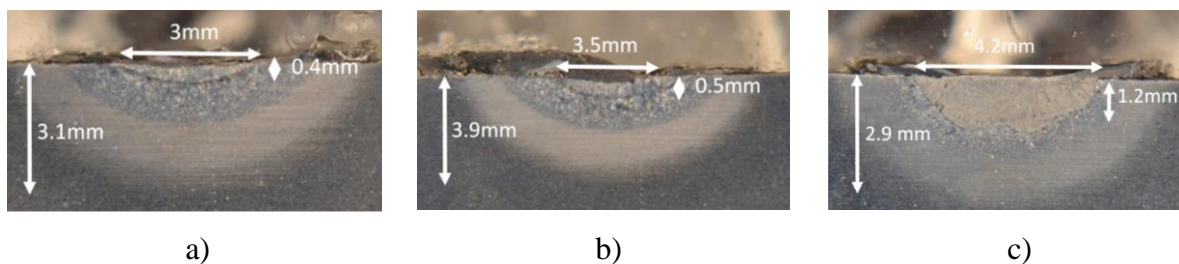

a)   b)   c)

Figure 4 - Dimensions of fusion zone for samples welded at 1.0 mm/s using argon as shielding gas a) E= 450J/mm, b) E= 500J/mm, and c) E= 600J/mm

Once again as expected, Figure 4 shows that the cross-sectional area increased with increased energy input; however, in this case, the concavity on the surface of the melted zone has decreased and a more homogeneous cross-sectional area was developed, especially when using E=600J/mm (Figure 3c). It is observe that when the energy input was increased by 33% (from 450 to 600 J/mm), the width increased 40% and the depth 200%, following more or less the same trend found for samples melted with argon at 0.5 mm/s. It must be highlighted that small deposits of un-melted material still remained on the surface on either side of the melt track.

Figure 5 summarizes the influence of the energy input on the cross-sectional area of the melted zone when using argon as shielding gas at different speeds
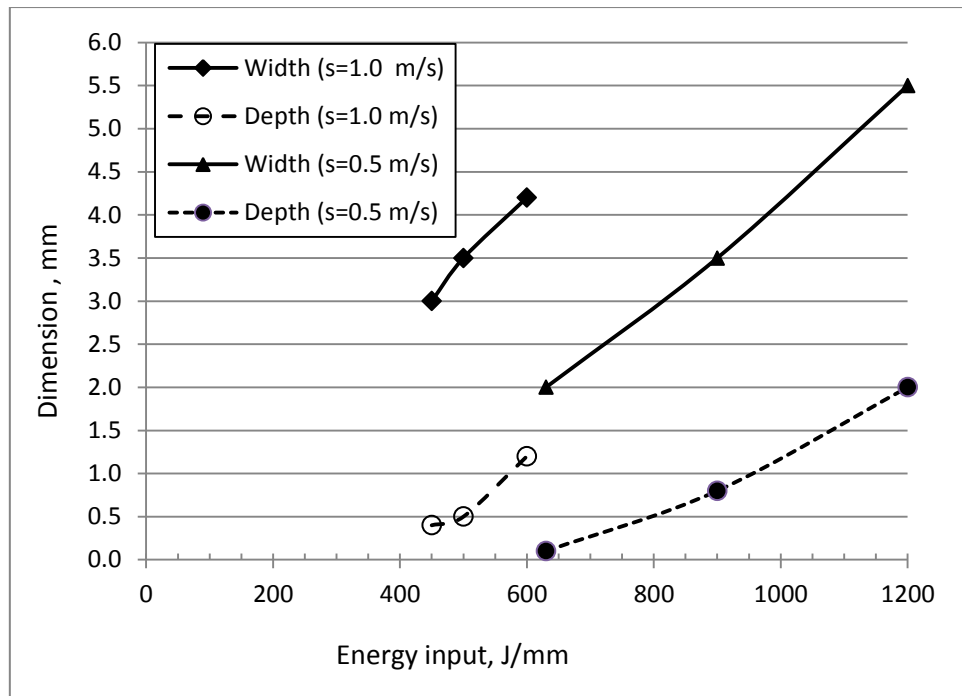
Figure 5. Cross sectional area dimensions of the melted zone vs energy input when melting with argon at different processing speeds

Analysing Figure 5 it is observed as previously explained, a deeper and wider fusion zone when heat input is increased independently of the processing speed; however it is also observed that for conditions ~600-630 J/mm, using a speed of 1.0 m/s seems to have a greater effect on the melted zone cross-sectional dimensions, as higher values of width and depth were registered. This result was not expected because decreasing the speed not only increases the energy input, as can be seen from equation 1, but also affects the contact time between the torch and the resultant melt zone dimensions. This gives more time for particles to melt, creating larger cross-sectional areas.

3.2 Argon + helium as shielding gas

Figures 6 and 7 show the cross-sectional area of the melted zone when using a mixture of argon + helium at different energy inputs and speeds of 0.5mm/s and 1.0 m/s respectively.
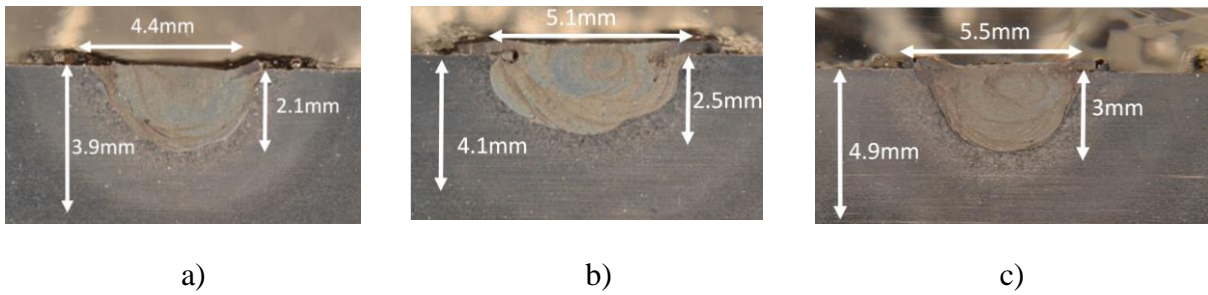
a)   b)   c)

Figure 6 - Dimensions of fusion zone for samples processed at 0.5mm/s using argon + helium as shielding gas a) E=900J/mm, b) E=1000J/mm, and c) E=1200J/mm
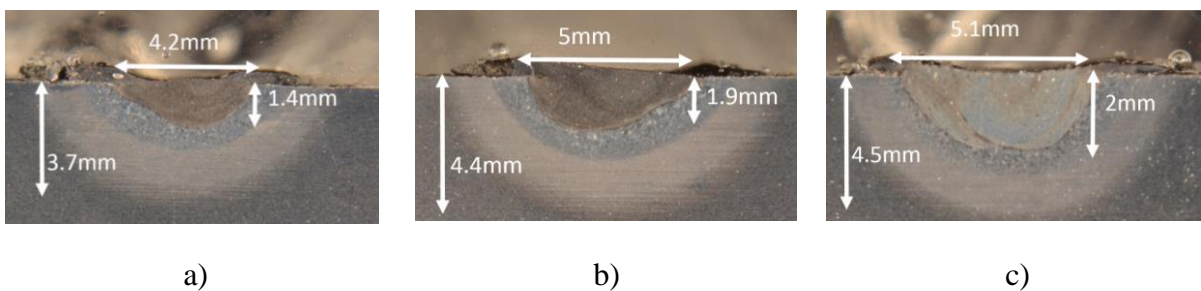

a)   b)   c)

Figure 7 - Dimensions of fusion zone for samples processed at 1.0 mm/s using argon + helium as shielding gas a) E=450J/mm, b) E=500J/mm, c) E=600J/mm

It can be observed in Figures 6 and 7, that as expected an increase in energy input produced an increase of the cross- sectional area of the melted zone.

Figure 8 is a graph comparing values of width and depth of the cross- sectional areas when using argon and argon + helium as shielding gas for 1.0 m/s
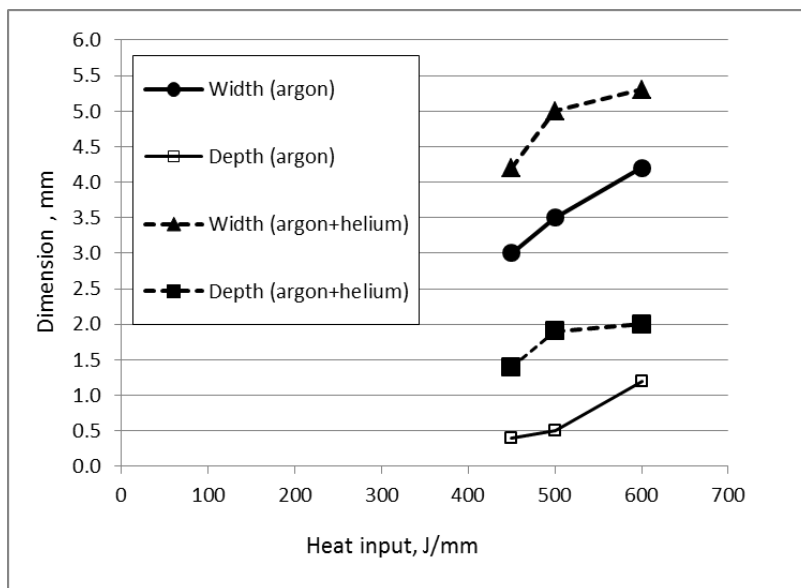

Figure 8 - Dimensions of fusion zone for samples processed at 1.0 mm/s
a) E=450J/mm, b) E=500J/mm, c) E=600J/mm

Samples melted with argon + helium developed a layer cross-sectional area under the same melting conditions. This was expected, due to the higher values of specific heat, thermal conductivity and first ionization potential provided by the helium. In general a 20% of addition of helium to the gas mixture produced a general increase of ~20% of the cross-sectional melted area. These results are in agreement with Tashira et al [8], where they suggest that the improvements observed when using an addition of helium are due to greater heat penetration into the parent material. It must be highlighted that some material still remains on the surface at either side of the re-solidified pool.

3.3 Microstructure

Figure 9 shows the parent microstructure of the microalloyed steel, where a ferritic phase (white zone) and pearlitic zone (dark zone) can be observed. As expected, the amount of pearlitic phase is small due to the small amount of carbon present in the alloy.
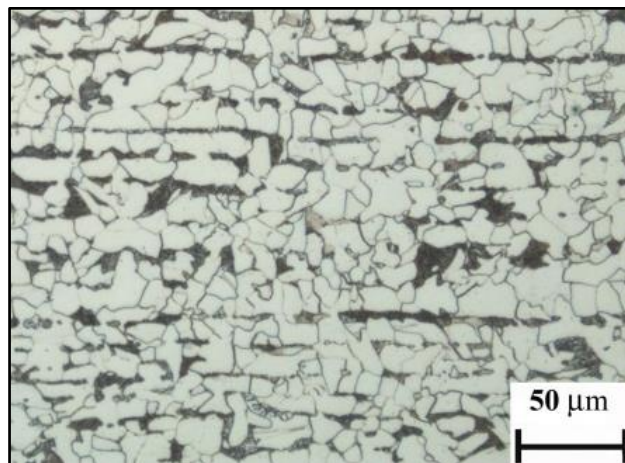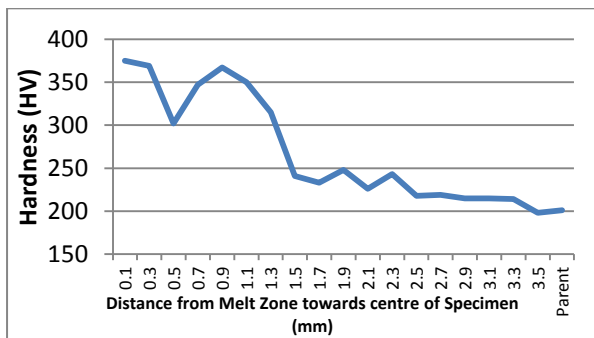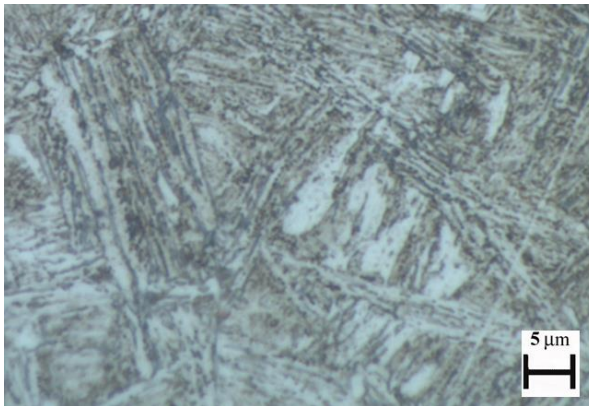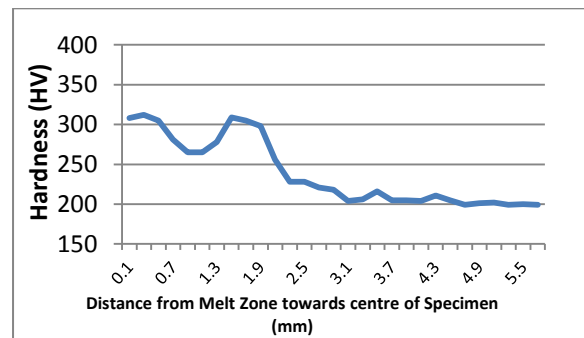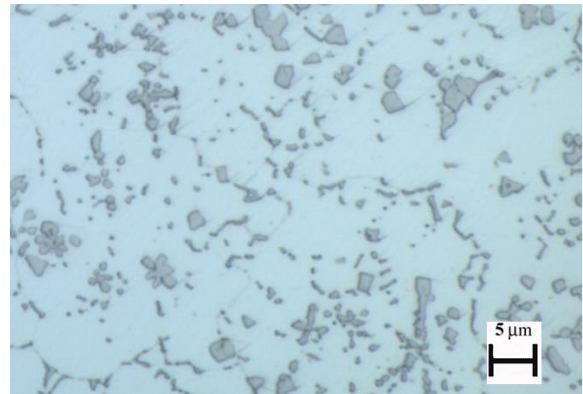

Figure 9. Microstructure of the parent material

Figure 10 shows images of the melted zone microstructure as well as the hardness profile of the cross sectional area.

Argon	**Argon + helium**

Figures 10. Microstructure and hardness and cross sectional area of samples melted using E=450J/mm and 1.0 m/s a) argon and b) argon+helium

Figure 10 shows, that in general , samples melted at energy inputs<600 J/mm under argon increased their hardness in the melted zone by ~75%, while samples melted with argon + helium increased their hardness by ~40%. This result is probably due to the fact that by adding helium to the mixture, higher temperatures were reached, leading to a decrease in the cooling rate and as a consequence the value of hardness.

Regarding samples melted at energy input of 1200J/mm and 0.5 mm/s, only a small increase of hardness was observed (~20%) using argon or argon + helium. This is again probably due to the fact that higher energy input produces higher temperatures which, as a consequence, achieves a slower cooling rate producing lower hardness ,Figure 10b. This is in agreement with the study Dyuti et al [9].
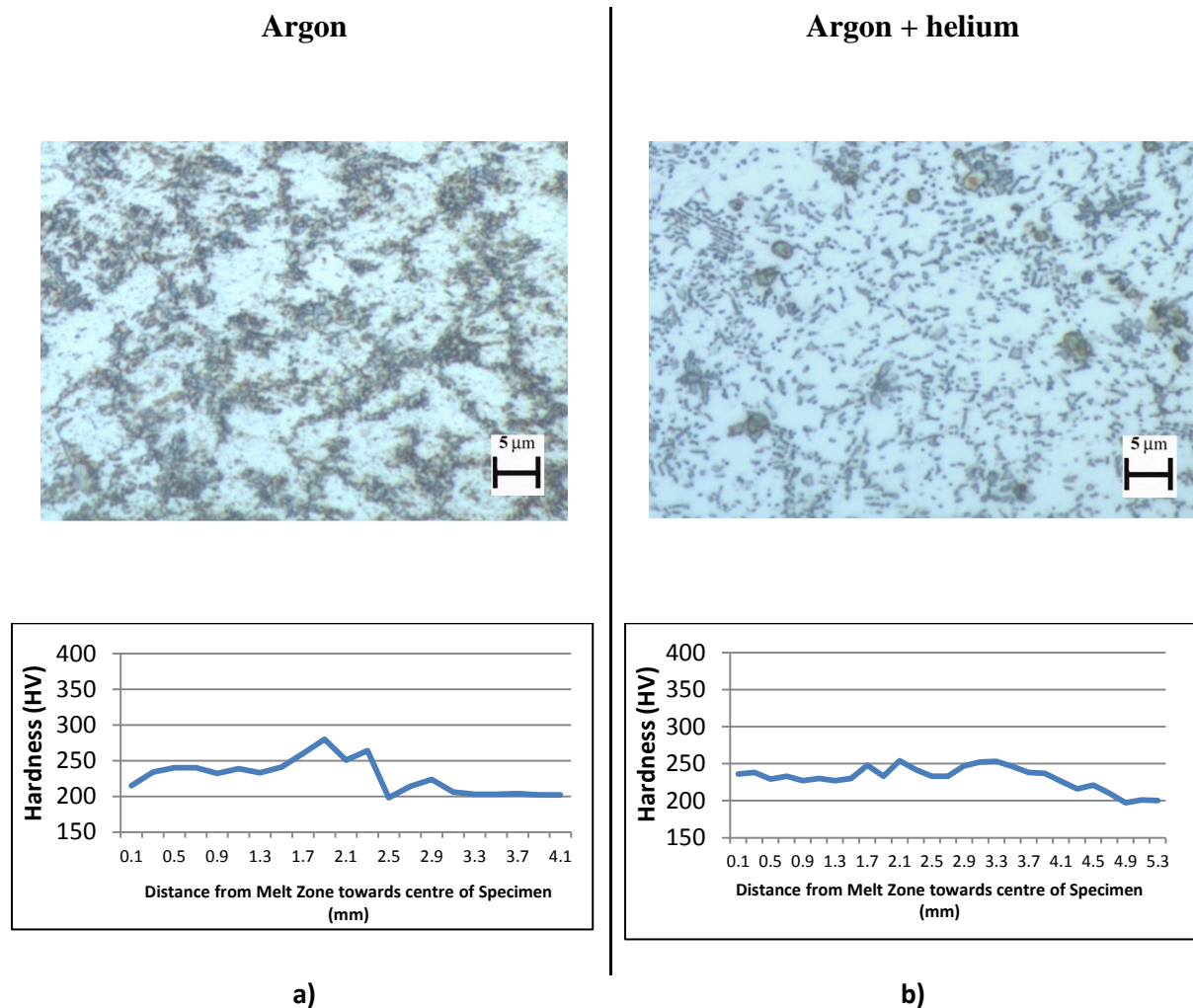
Argon	Argon + helium

Figure 11. Microstructure and hardness and cross sectional area of samples melted using E=1200J/mm and 0.5 m/s a) argon and b) argon + helium

It is observed that for energy input≤ 600 J/mm, Fig. 10, the microstructure of the melted zone is martensitic when using argon as shielding gas, while coarser grains are observed when using energy input of 1200 J/mm, Figure 11. However, using a mixture of argon + helium, the microstructure for all energy inputs is similar to a grey cast iron .

Figure 12 shows the X-ray diffraction results, where the lowest spectrum corresponds to the as- received powder. This clearly shows peaks from Ti_2AlC, but also peaks from Ti_3AlC_2 and TiC. The other spectra in this figure were obtained from the surfaces of samples which had been TIG processed with argon as a shielding gas, and with a range of energy inputs increasing moving up the figure. 450J/mm processing resulted in a breakdown of the powder constituents except TiC, which showed stronger peaks than in the powder. Also, both small quantities of iron titanium and aluminium iron titanium, with a suspicion of aluminium oxide.
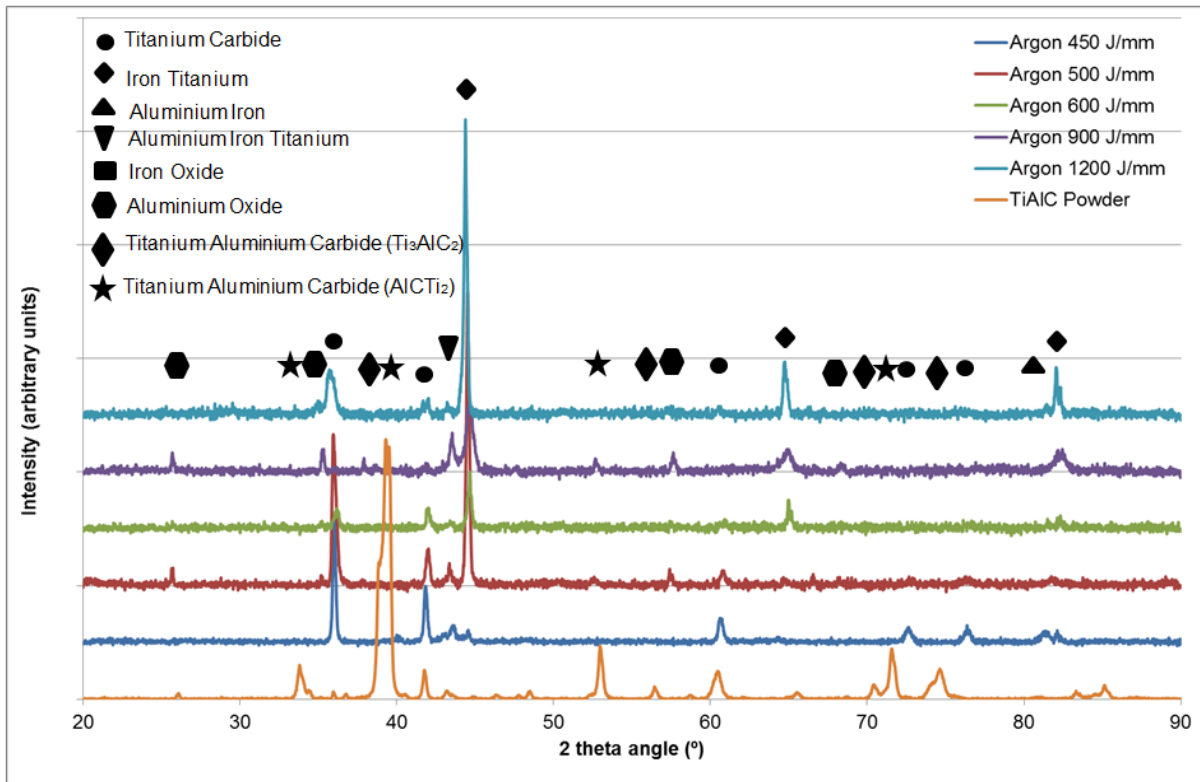
Figure 12. X-ray diffraction spectra for Ti_2AlC powder and from sample's surface melted with at different energy input.

The TiC peaks decreased with increasing energy inputs above 500J/mm, while the iron titanium peaks increased. After 1200J/mm processing, the strongest peaks present corresponded to iron titanium with TiC. It is of interest to note that Al_2O_3 if formed when Ti_2AlC is heated above 1450°C, when it decomposes TiC [3].

The SEM EDX spectra recorded between the surface to the steel substrate showed that titanium and aluminium were only found within the melt zone, all traces of the ceramic particles being lost in the HAZ. Titanium is present in the first 100 μm below the melt zone surface, and again is significant in the melt zone just above the MZ/HAZ interface as observed in Figure 13.
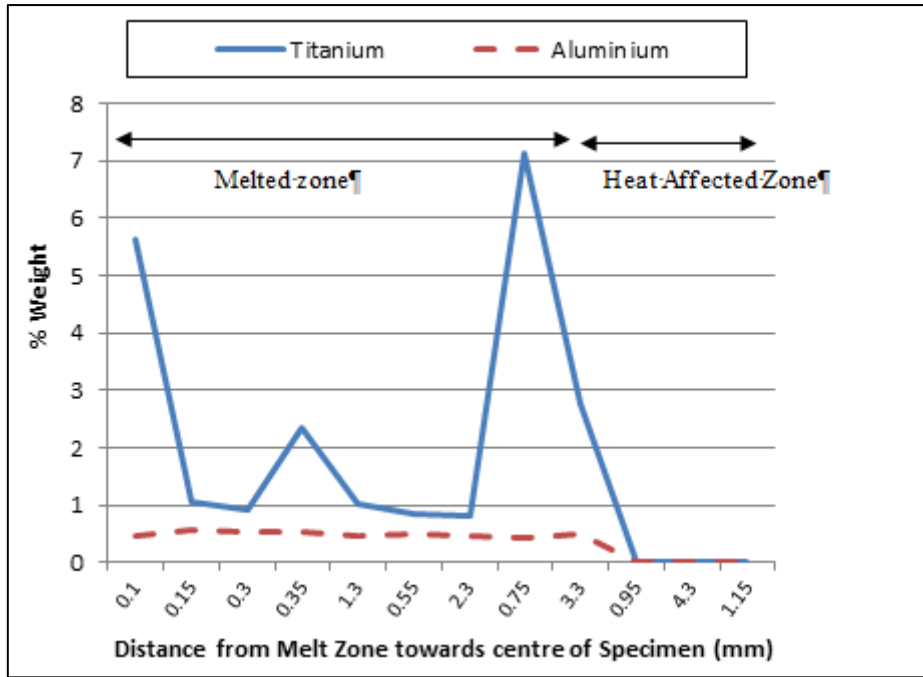
Figure 13. Distribution of titanium and aluminium across different zones of sample melted using a 500J/mm and argon as shielding gas

The corresponding information for the argon + helium using an energy input of 900J/mm and a welding speed of 0.5 m/s, is given in Figure 14. Here, four peaks occur for Ti within the melt zone , along with a small amount of aluminium.
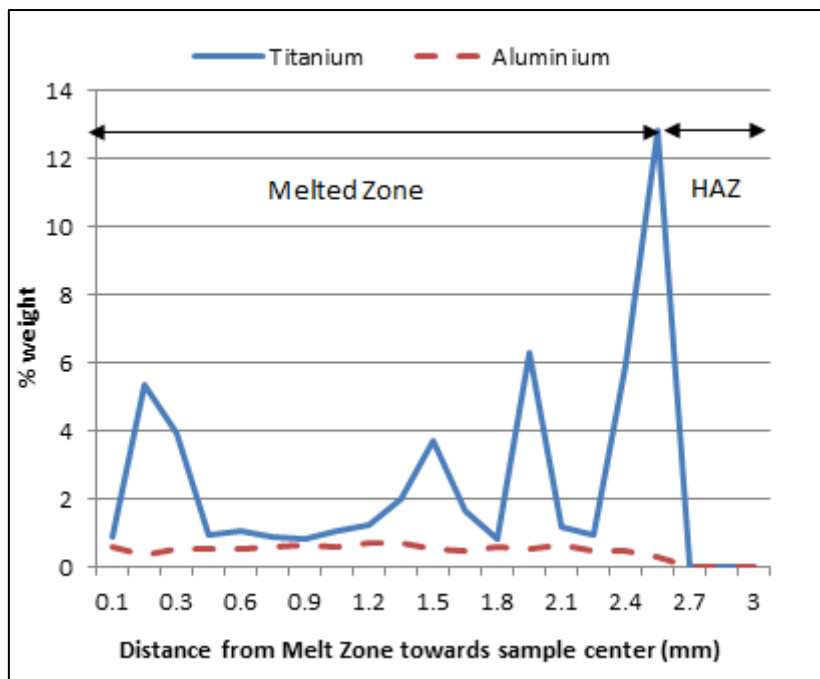

Figure 14 - Distribution of Titanium and Aluminium across different zones of sample melted with 900J/mm using argon + helium as shielding gas

To determine if a correlation existed between hardness and distribution of aluminium and titanium within the melted zone of each of the successfully melted samples, further SEM analysis were carried out and Figure 16 shows these results. The titanium peaks observed in the melt zones of Figures.13 and 14, were studied further with the argon + helium 500J/mm sample. In conjunction with Fig.15, the peaks are shown to correspond to areas in the SEM micrographs from three positions within the melt zone containing rounded particles, coinciding with peaks in hardness. These are also areas showing high concentration of titanium, which the lines in the spectra in Figure 12 confirm, are most likely due to TiC.
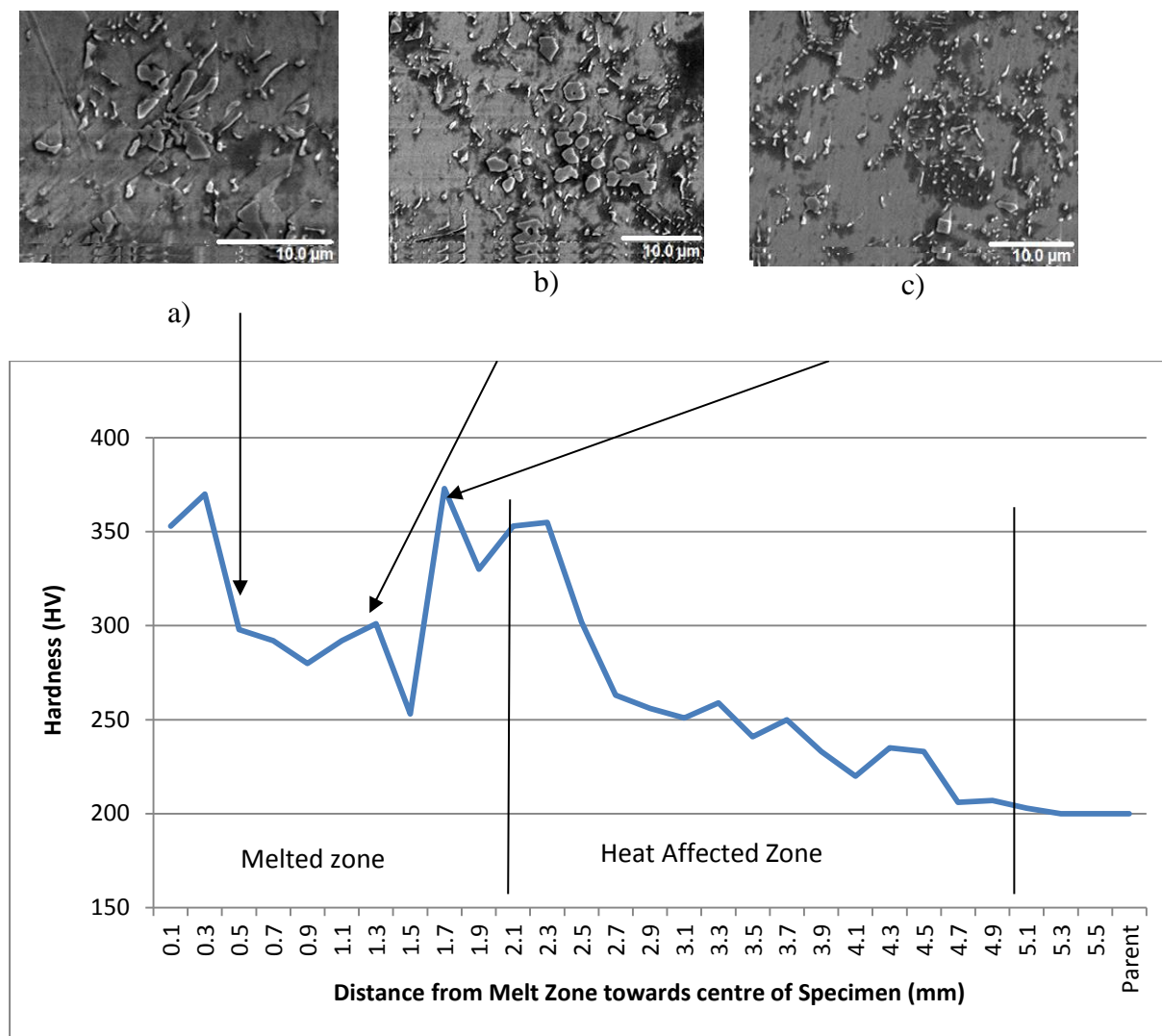

Figure 15. SEM images of titanium containing particles within 500J/mm sample using argon + helium from: a) beginning of melted zone, b) middle of melted zone, c) end of melted zone at X5000 magnification

Furthermore, SEM analysis on the sample processed at 900J/mm using argon + helium gas, was extended by observing the changing microstructure within the heat affected zone, as hardness decreases during its transition back to the parent material.
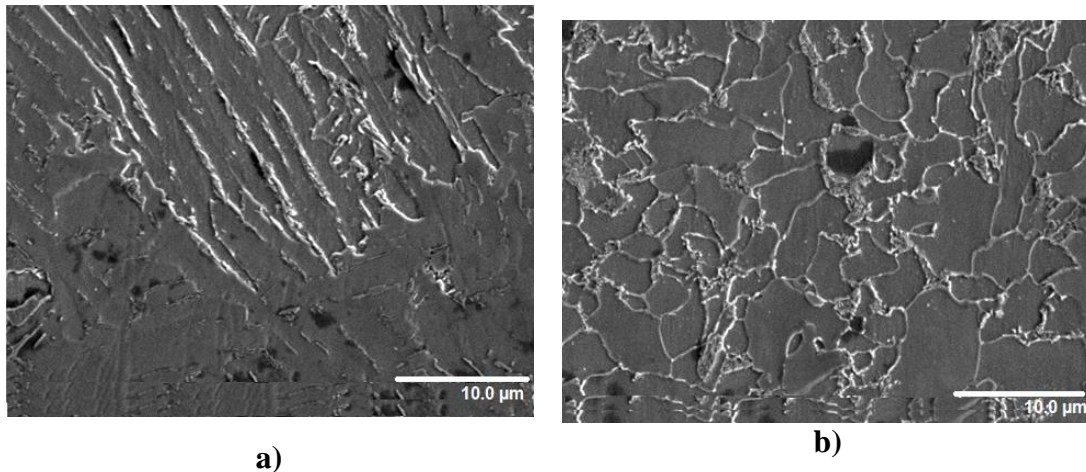

a)

b)

Figure 16 – SEM image of sample melted with 900J/mm using argon + helium, a) heat affected zone, b) transition between heat affected zone and parent material

Figure 16a shows needles typical of lath structure within the microstructure of the heat affected zone of the sample melted with 900J/mm using argon + helium gas. This microstructure corresponds to the still fairly higher values of hardness found within this region. In Fig. 16b. a microstructure intermediate between a fully developed MA steel substrate ferrite/pearlite microstructure can be seen. Here, ferrite grains, have possibly small particles of cementite nucleated on their boundaries. It would appear that a contribution to the higher hardness associated with the MZ/HAZ is due to the martensitic- like microstructure.

The SEM analyses confirms that the Ti_2AlC powder decomposed and that TiC particles were distributed throughout the melted zone in each of the samples analysed. It should be noted that while hardness was used for correlating with the microstructure, the incorporation of Ti_2AlC within the surface of an microalloyed steel would not be envisaged as a means of improving wear resistance, as it is not as hard as TiC and more expensive, and is therefore does not provide an economic route. However, of methods and process conditions can be found to retain Ti_2AlC with a steel surface, its other advantages can be developed.

4. Conclusions

Several conclusions and recommendations can be drawn from this research :

- In general, after TIG processing using argon the resolidified showed smaller cross-sectional areas compared to argon + helium, but had an increase of hardness of ~75%; a more homogeneous cross- sectional area was obtained when using argon + helium.

- Overall best conditions to achieve a homogeneous and hard cross sectional area seems to be when using argon, energy input=600 J/mm and v=1.0 mm/s.

- SEM/EDX and XRD analyses confirmed that Ti_2AlC particles decomposed to TiC particles within the melt zone, resulting in an increase in hardness.

Further experimental work is necessary to find the optimum conditions to avoid Ti_2AlC decomposing during TIG processing thereby enabling the creation of a surface composite on steel, showing good oxidation resistance.

5. References

1 D.B. Miracle. Metal matrix composites – From science to technological significance. Composites Science and Technology 2005;65:2526–40.

2 R.E. Smallman and A.H.W. Ngan. Oxidation, Corrosion and Surface Engineering. Modern Physical Metallurgy 2014:617-57.

3 Michel Barsoum and Miladin Radovic. MAX Phases: Bridging the gap between metals and ceramics. American Ceramic Society Bulletin. 2014; 92,20-27

4 M.J. Zhuo, Z.J. Lin, Y.C. Zhou , M.S. Li , J.Y. Wang - Microstructural characterization of layered ternary Ti2AlC. 2005.

5 MEI Bing-chu, WANG Ping, HONG Xiao-lin, ZHOU Wei-bing Synthesis of Ti2AlC by hot pressing and its mechanical and electrical properties. 2007.

6 W.K.Pang,I.M.Low,B.H.O'Connor,A.J.Studer,V.K.Peterson,Z.M.Sun and J-P Palmquist, Comparison of thermal stability in MAX211 and 312 phases',J.Phys.,Conf.Ser.,vol.251,(2010), 012025,1-5.

7 K. Weman. Welding Processes Handbook – TIG WELDING. 2012.

8 S. Tashira, M. Tanaka, T. Satoh, A. B. Murphy and J. J. Lowke Influence of shielding gas composition on arc properties in TIG welding. 2007.

9   S. Dyuti, S. Mridha and S. K. Shaha, Formation of Ti-Al-N Dispersed Layer on Steel Surface by TIG Melting in a Reactive Environment, *Advanced Materials Research Vols. 264-265 (2011) pp 1433-1438,*

10 S.Hashimoto, M. Takeuchi, K. Inoue, S. Honda, H. Awaji, K. Fukuda and S. Zhang. Pressureless sintering and mechanical properties of titanium aluminum carbide. Materials Letters 2008;62:1480-3.

11 L. Shi, J. Zhang, L. Wang, W. Jiang and L. Chen) Fabrication, Microstructure and Mechanical Properties of TiC/Ti2AlC/TiAl3 in situ Composite, J. Mater. Sci. Technol., 2011, 27(3), 239-244.